Following the Molecular Mechanism for the NH3 + LiH → LiNH2 + H2 Chemical Reaction. A Study based on the joint use of the Quantum Theory of Atoms in Molecules (QTAIM) and Non-coval...

ARTICLE *in* THE JOURNAL OF PHYSICAL CHEMISTRY A · FEBRUARY 2014

Impact Factor: 2.69 · DOI: 10.1021/jp4111376 · Source: PubMed

4 AUTHORS, INCLUDING:

Julia Contreras-García
Pierre and Marie Curie University - Paris 6
54 PUBLICATIONS **1,439** CITATIONS
SEE PROFILE

Patricio Gonzalez-Navarrete
Technische Universität Berlin
20 PUBLICATIONS **181** CITATIONS
SEE PROFILE

THE JOURNAL OF PHYSICAL CHEMISTRY A

Article

pubs.acs.org/JPCA

Following the Molecular Mechanism for the $NH_3 + LiH \rightarrow LiNH_2 + H_2$ Chemical Reaction: A Study Based on the Joint Use of the Quantum Theory of Atoms in Molecules (QTAIM) and Noncovalent Interaction (NCI) Index

Juan Andrés,*[,†] Slawomir Berski,[‡] Julia Contreras-García,[§,∥] and Patricio González-Navarrete[†]

[†]Departament de Química Física i Analítica, Universitat Jaume I, 12071 Castelló, Spain

[‡]Faculty of Chemistry, University of Wroclaw, 14 F. Joliot-Curie, 50-383 Wroclaw, Poland

[§]Laboratoire de Chimie Théorique, Sorbonne Universités, UPMC Univ Paris 06, UMR 7616, F-75005 Paris, France

[∥]CNRS, UMR 7616, LCT, F-75005 Paris, France

Supporting Information

ABSTRACT: The molecular mechanism for the $NH_3 + LiH \rightarrow LiNH_2 + H_2$ reaction has been elucidated by the combined use of quantum theory of atoms in molecules (QTAIM) and noncovalent interactions (NCI) index. The topology of the electron density, obtained by QTAIM/NCI, is able to identify the evolution of strong and weak interactions, recovering the bonding patterns along the reaction pathway. Thus, the combination of these two techniques is a useful and powerful tool in the study of chemical events, providing new strategies to understand and visualize the molecular mechanisms of chemical rearrangements. Also, for the first time, the topology of the reduced density gradient has been analyzed, taking into account saddle points for the construction of bifurcation trees. This approach has demonstrated the ability of NCI to account for delocalized interactions, very often characteristic of transitions states.

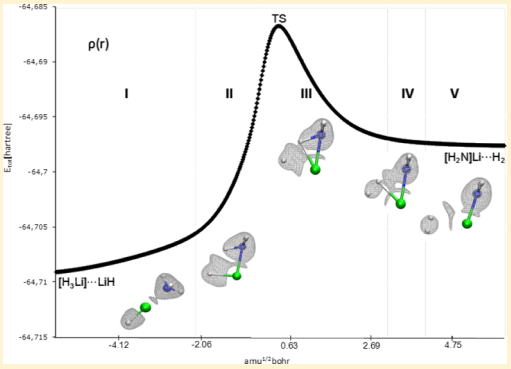

1. INTRODUCTION

Revealing the chemical bonding (structure) and the reorganization of the chemical bonds (reactivity) of any chemical transformation forms the undisputed foundation of chemistry.[1,2] Chemical reactions, in general, essentially manifest rearrangements of their nuclei, which are directly related to the forming/breaking bond processes along the reaction; therefore, understanding a chemical process requires in essence the knowledge of its molecular mechanism. For its part, the reaction mechanism corresponds to the mapping of the atoms from reactants to products, identifying not only the nature of the changing atoms but also the sequence of breaking and making of bonds between them. Detailed insight into the molecular mechanism of a chemical reaction requires the knowledge of how the properties of the reactants change along a representative reaction path to yield the product via the corresponding transition state (TS) or possible intermediates, as well as an accurate description of the electronic structure. Such knowledge is seldom complete and implies continuous changes of the molecular structure.

Chemical bonds are not directly observable; however, an adequate representation as well as the description of the bond breaking/forming processes should be provided by a physical observable defined in coordinate space. The electron density, $\rho(r)$, meets these requirements because it is an experimental accessible scalar field, which is a local function defined within the exact many-body theory, and supported by the Hohenberg–Kohn theorem (HKT).[3] The relationship between charge density topology and physical/chemical properties can be understood from the HKT as it asserts that a system's ground-state properties are a consequence of its charge density.[3] Since chemical reactions proceed by $\rho(r)$ redistributions, the methods that deal with the analysis of the $\rho(r)$ distribution should have a particular appeal for chemists and help to understand the electron structure of molecules and thus chemical reactivity. To describe adequately these properties of chemical reacting systems, additional tools for extracting observable information are necessary. This is achieved by Bader's Quantum Theory of Atoms in Molecules (QTAIM), a model based on quantum mechanics and physical observables, providing a rigorous and exact definition of bonding within an atomic ensemble in terms of topological properties of its charge density.[4] Thus, a molecular mechanism of a given chemical reaction can be studied from the redistribution of the electron density along the reaction path connecting the stationary points. Bader and coworkers pioneered the study of the structural change based on

Received: November 12, 2013
Revised: February 4, 2014
Published: February 5, 2014

the electron density using Thom's theory of elementary catastrophes.[5] Likewise, the topological analysis of the electronic localization function (ELF),[6−8] $\eta(r)$, is becoming increasingly popular in the characterization of chemical bonding in systems ranging from clusters in the gas phase to solids. In this sense, Silvi and co-workers have developed the bonding evolution theory (BET) as a generalization of Bader's work and to other scalar fields as ELF.[9,10] Several research groups have used the electron density,[11−14,58] its Laplacian,[15,59] ELF,[16−22] and electrostatic potential[23,24] to study molecular mechanisms or conformational changes of several systems using these approaches.

Alternatively, noncovalent interactions are of critical importance in many chemical, biological, and technological systems. Protein−ligand interactions,[1,2] self-assembly of nanomaterials,[25,26] folding of proteins,[27,28] and packing of molecular crystals[29] are controlled by a delicate balance of numerous weak noncovalent interactions. Apart from $\rho(r)$ and $\eta(r)$, one of us recently introduced a new approach to visualize noncovalent interactions. The noncovalent interactions (NCI)[30−32] index enables the study of domains of the electronic density associated with weak interactions that exhibit both low electron density and low reduced density gradient $s(\rho)$. The reduced density gradient $s(\rho)$ is defined using the electron density and its gradient:

$$\frac{1}{2(3\pi^2)^{1/3}}\frac{|\nabla\rho(r)|}{\rho(r)^{4/3}} \tag{1}$$

where $\rho(r)$ is the electron density. It is a dimensionless quantity used in density functional theory to describe the deviation from a homogeneous electron distribution. In density tails (i.e., regions far from the molecule, in which the density is decaying to zero exponentially), the reduced gradient has very large positive values. On the contrary, the $s(\rho)$ function assumes very small values, approaching zero, for regions of both covalent bonding and noncovalent interactions. By multiplying the density by the sign of the second eigenvalue of the density Hessian (λ_2), one can distinguish the strength and the attractive or repulsive nature of the interactions.[33] A characterization of places where the noncovalent interactions play an essential role in a molecule stems from the experimental observations that such interactions may be responsible for the course of the chemical reactions. For instance, the rupture of the covalent carbon−carbon bond[34] and the formation of alkane nanostructures that are covalently bound to silicon surfaces occurs thanks to dispersion interactions.[35] The density critical point (CP) that occurs between weak inter- or intramolecular interactions induces dramatic changes in the $s(\rho)$ plot. Since the behavior of $s(\rho)$ at low densities is dominated by $\rho(r)$, $s(\rho)$ tends to diverge except in the regions around a density CP, where the density gradient dominates, and $s(\rho)$ approaches zero. When we search for the points in real space giving rise to this feature, the noncovalent region clearly appears in the (supra)molecular complex. Indeed, very recently, across QTAIM/NCI analysis in solids has shown to provide a deeper insight into the nature of interactions in solids,[36] whereas the cross ELF/NCI analysis has been presented to offer an alternative look of chemical mechanisms for prototypical organic reactions.[37]

Taking into account this theoretical background, the purpose of this article is the study of the evolution of atomic interactions for the $NH_3 + LiH \rightarrow LiNH_2 + H_2$ reaction by means of the electron density[38] and the newly proposed and especially suited for noncovalent interactions, reduced density gradient $s(\rho)$ function.[32] This reaction is a challenging example where both ionic (Li^+ H^-) and covalent (H−H) bonds as well as van der Waals interactions (N···LiH) are present along the chemical process. While an accurate analysis together with a strict definition of breaking/forming process is required in order to gain an accurate description of this chemical transformation, the combined use of the $\rho(r)$ and $s(\rho)$ field functions might provide further insights into the molecular mechanism.

Because of its high electrochemical potential, lithium is used in several types of applications and particularly in the production of batteries, which are especially important for electric vehicles and aerospace applications. In particular, Chen et al.[39] have demonstrated that lithium nitride can reversibly take up large amounts of hydrogen by means of the following reaction path:

$$Li_3N + 2H_2 \leftrightarrow Li_2NH + LiH + H_2 \leftrightarrow LiNH_2 + 2LiH \tag{2}$$

Likewise, Hu and Ruckenstein[40,41] demonstrated that another ultrafast reaction between the ammonia and lithium hydride $NH_3 + LiH \rightarrow LiNH_2 + H_2$ may be responsible for generation of ammonia during the hydrogenation of Li_3N and decomposition of the hydrogenated Li_3N. This reaction has been previously studied using second-order perturbation theory (MP2) and coupled cluster CCSD(T) theory with aug-cc-pVTZ basis set by Kar et al.,[42] whereas one of us has studied the reaction pathway taking into account the topological analysis of the $\eta(r)$ and $\rho(r)$ fields.[43]

The article is organized as follows: first, results of topological analysis of $\rho(r)$ are presented; evolution of atomic interactions achieved from analysis of $s(\rho)$ distribution is described next. It should be noted that it will be the first time that the topology of $s(\rho)$ has been analyzed, taking into account not only its sinks[44] but also the saddle points for the construction of bifurcation trees. This approach will show the ability of NCI to account for delocalized interactions, very often characteristic of TSs. Finally, the results achieved using both scalar fields are compared.

2. COMPUTATIONAL DETAILS

The optimization of geometrical structures, generation of the intrinsic reaction coordinate (IRC) path, and wave function files for the topological analysis have been performed using Gaussian09 (G09) program.[45] The standard B3LYP electron density functional[46−48] and the aug-cc-pVTZ basis set[49] have been used. The localization of the energy minimum on the potential energy surface (PES) for the $H_3N\cdots Li^+H^-$ complex (C_{3v}) has been verified by means of vibrational analysis that did not yield any imaginary frequencies. In the case of the product complex, $H_2NLi\cdots H_2$, problems with small imaginary frequencies were detected (<30 cm^{-1}), and therefore, the symmetry of the C_{2v} point group has been imposed. The TS of the reaction has been identified by means of one imaginary frequency (1071.2i cm^{-1}) and verified with the IRC procedure. The activation energy has been calculated including zero-point vibrational corrections.

The IRC calculations have been performed using the Hessian based predictor−corrector method proposed by Hratchian and Schlegel[50] and implemented in G09. The minimum on the PES going from the TS to the $H_2NLi\cdots H_2$ complex has been found after 270 points and 267 points going to the $H_3N\cdots LiH$

dx.doi.org/10.1021/jp4111376 | J. Phys. Chem. A 2014, 118, 1663−1672

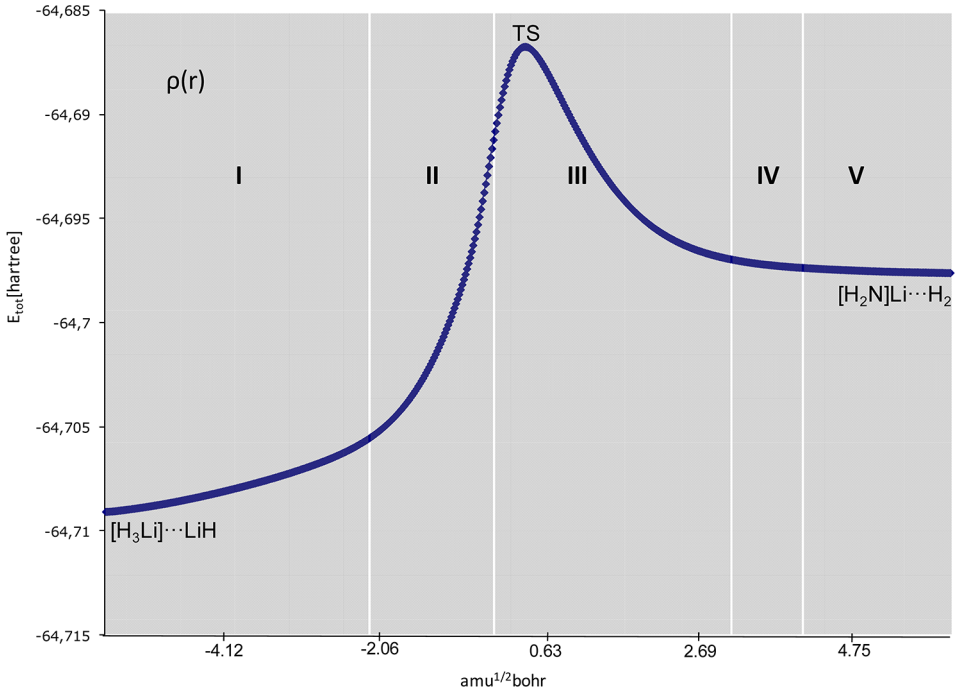

Figure 1. IRC path with marked structural stability domains obtained from the topological analysis of $\rho(r)$. The activation energy of the process is predicted to be 7.59 kcal/mol.

complex. The step size along the reaction path (Rx) has been set to 0.02 amu$^{1/2}$ bohr.

The topological analysis of the $\rho(r)$ and $s(\rho)$ functions have been performed for each point on the IRC path. In the case of $\rho(r)$ distribution, the AIMall program[51] of Keith with standard thresholds has been used. For each studied point on the IRC pathway, the number of the localized CPs fulfilled the Poincaré−Hopf condition. In comparison to the previous results[43] achieved using the ext94b program[52] some differences have been found. They are associated with the bond paths since, depending on used software, they terminate at one or another of the hydrogen atoms of the dihydrogen molecule.

The NCI analysis has been carried out using to the NCIPLOT code.[31] The bifurcation points and reaction steps have been determined in a visual manner using the VMD software[53] for grids calculated with an accuracy of 0.1 Å along each axis. Although the complete topological analysis has not been carried out for this field (i.e., the complete list of CPs have not been determined), the visual approach easily enables to pinpoint the relevant crossing points and their bifurcation values. For details concerning the analysis of the reduced density gradient index, please see refs 30−33.

3. RESULTS AND DISCUSSION

(a). Topological Analysis of the Electron Density, $\rho(r)$.

The topological analysis of $\rho(r)$ field reveals that the H_3N + LiH → H_2NLi + H_2 chemical reaction presents five different topological domains separated by their respective bifurcation points. Figure 1 shows the energy profile as well as the different steps (topological domains) involving the chemical process. The evolution of the values of $\rho_{(3,-1)}(r)$ and $\nabla^2\rho_{(3,-1)}(r)$ computed for selected (3,−1) bond critical points during the studied reaction is presented in Figure 2.

In the first step, the $Li^+H_b^-$ bond bends toward the N−H_a bond. The separation between the H_a and H_b atoms decreases from 4.13 to 2.24 Å, while the distance between $Li^+H_b^-$ bond is

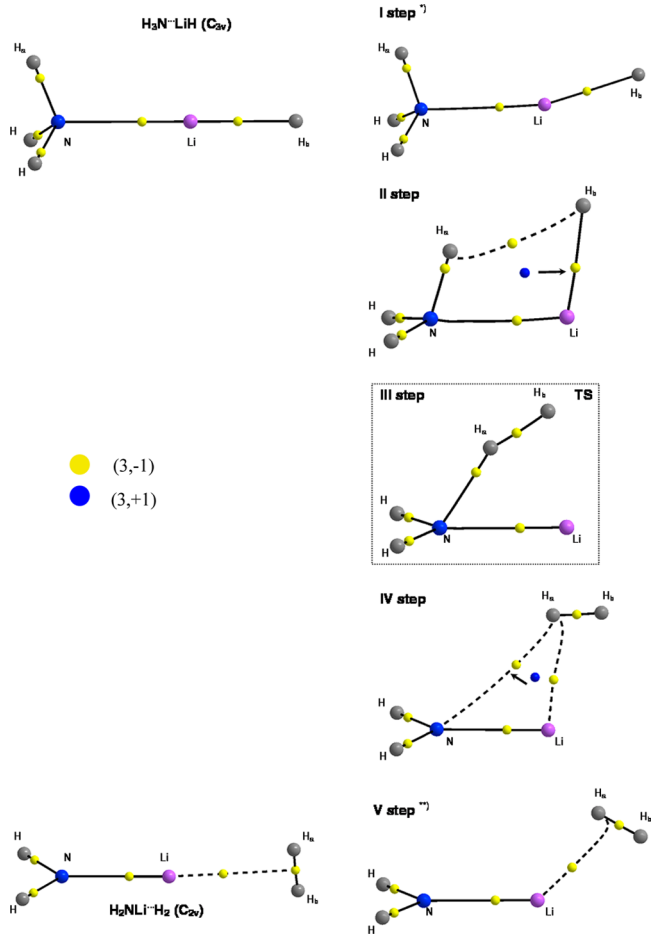

Figure 2. Evolution of the CPs for the electron density field. The marks * and ** correspond to first and last points on the IRC path, respectively.

dx.doi.org/10.1021/jp4111376 | J. Phys. Chem. A 2014, 118, 1663−1672

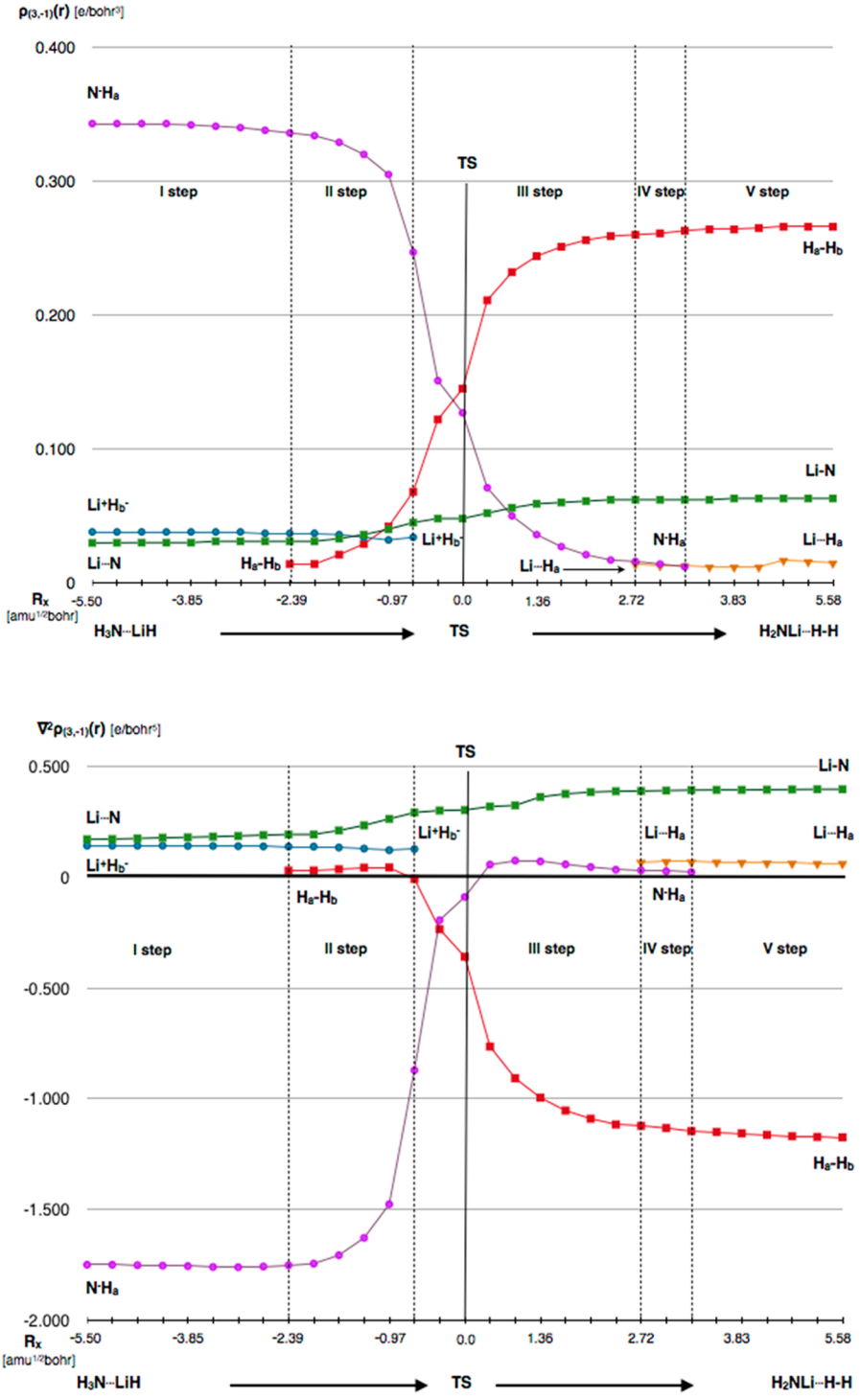

Figure 3. Evolution of the $\rho(r)$ and $\nabla^2\rho(r)$ field along the IRC path at some specific (3,−1) CPs.

elongated from 1.61 to 1.64 Å. This step contains 160 points on the IRC path, where the values of $\rho_{(3,-1)}(r)$ and $\nabla^2\rho_{(3,-1)}(r)$ do not change substantially along this stage.

The first fold type catastrophe is observed for the second step of the reaction (79 points on the IRC path) at Rx ≈ −2.204 amu$^{1/2}$ bohr. Two new (3,−1) and (3,+1) CPs are localized in the region between the H_a atom from the ammonia and the H_b atom from the lithium hydride ($H_a\cdots H_b$). The change of the $\rho(r)$-topology is caused by mutual bending of the N−H_a and $Li^+H_b^-$ fragments that results in the decreasing of the $H_a\cdots H_b$ distance. In this step the value of $\rho_{(3,-1)}(r)$ for the N−H_a bond gradually decreases, while the value of $\nabla^2\rho_{(3,-1)}(r)$ becomes less negative. In the case of the (3,−1) CP localized in the $H_a\cdots H_b$ region, their respective values of the electron density and Laplacian increase. In other words, along the first step, the N−H_a bond decreases its covalency as the $H_a\cdots H_b$ bond gets slightly stronger. The analysis of all points on the IRC path in the second step shows that the (3,+1) CP approaches to the (3,−1) CP that characterizes the ionic interaction between the Li and H_b atoms (see Figure 2).

The second-fold type catastrophe is localized at Rx ≈ −0.557 amu$^{1/2}$ bohr. The fold determines the $\rho(r)$ topology in the third

dx.doi.org/10.1021/jp4111376 | J. Phys. Chem. A 2014, 118, 1663−1672

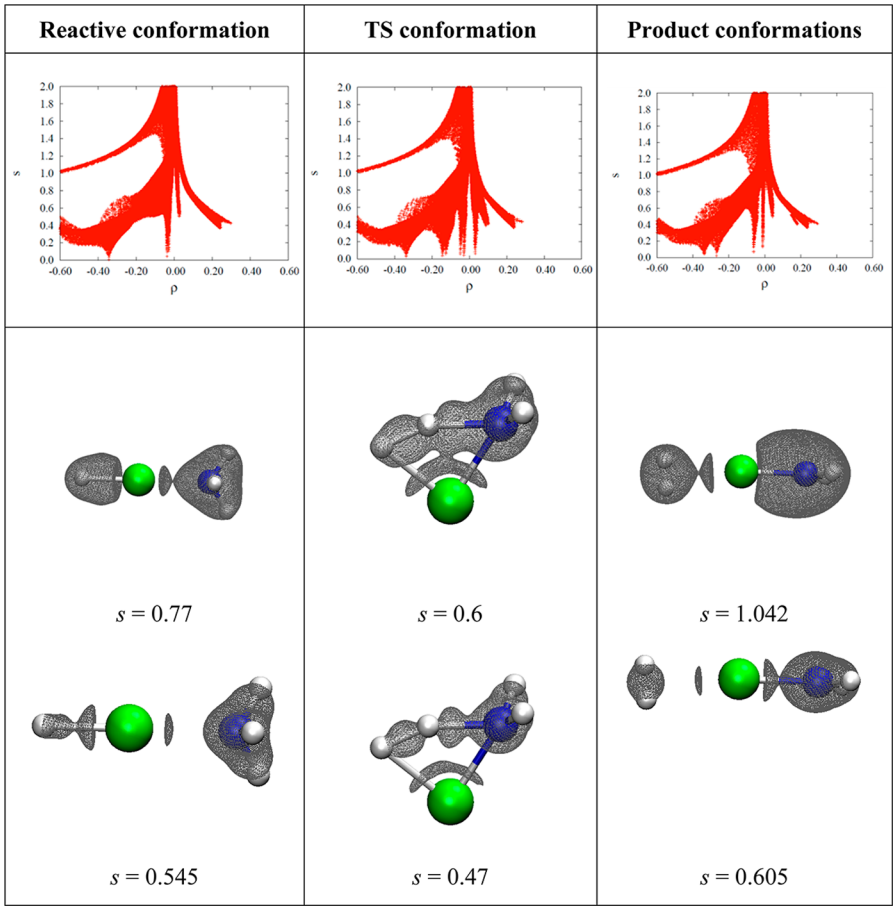

Figure 4. Plots of the reduced density gradient versus the electron density multiplied by the sing of the second Hessian eigenvalue $\rho(r)(\lambda_2)$; for reactive, TS, and product as well as their respective reduced gradient isosurfaces. The importance of pseudopeaks is highlighted by representing several isosurface values.

step. The (3,+1) and (3,−1) CPs, which were involved in the $Li^+H_b^-$ interaction, are annihilated. From the topological point of view, the lithium−hydrogen interaction of the ionic type is broken. The reacting system constitutes now the $H_b\cdots H_a\cdots N(H_2)\cdots Li$ complex formed by the covalently bound NH_2 fragment interacting with the Li atom and the $H_b\cdots H_a$ unit. This step contains 160 points on the IRC path. It is worth noting that at Rx ≈ −0.557 $amu^{1/2}$ bohr the character of the $H_a\cdots H_b$ interaction changes because the Laplacian value for (3,−1) CP switches from positive to negative (see Figure 3). The negative sign of $\nabla^2\rho_{(3,-1)}(r)$, typical for the shared interactions, is expected for the covalent H_a-H_b bond at the end of the reaction. The $H_a\cdots H_b$ distance shortens in this step, and the value of electron density subsequently rises and the Laplacian becomes more negative. An opposite behavior is observed for the $N\cdots H_a$ interaction. The shorter $N\cdots H_a$ distances correspond to the smaller values of $\rho_{(3,-1)}(r)$ and less negative values of $\nabla^2\rho_{(3,-1)}(r)$. The qualitative change of the $N\cdots H_a$ interaction is observed at Rx ≈ 0.227 $amu^{1/2}$ bohr where the Laplacian value becomes positive. The third step contains the TS, as shown in Figures 1 and 2, but it is not possible to find any qualitative change of atomic interactions for this point.

The third-fold catastrophe is observed after the TS at Rx ≈ 2.720 $amu^{1/2}$ bohr. The fold results in the formation of two new (3,+1) and (3,−1) CPs localized approximately between the Li and H_a atoms. The new (3,−1) CP lies on the gradient path joining the Li with H_a nuclear attractors. From the topological point of view, the appearance of the (3,−1) CP may be interpreted as the origin of the interaction between the lithium and hydrogen (H_a) atoms. The Laplacian value for the (3,−1) CP is slightly positive indicating noncovalent interactions. The fourth step is found for 45 points on the IRC path. The analysis of the geometrical structures for this step shows that the (3,+1) CP moves toward the (3,−1) CP lying on the gradient path joining the N and H_a nuclear attractors.

The last fold catastrophe is found at Rx ≈ 3.648 $amu^{1/2}$ bohr. The critical point (3,+1) and the critical point (3,−1) localized on the gradient path joining the N nuclear attractor with the H_a nuclear attractor are annihilated. From the topological point of view, there is no more indication of the interaction between the N and H_a atoms. The electronic structure of the reacting system is now similar to that one observed for the $H_2NLi\cdots H_2$ complex optimized for the minimum of the total energy. The (3,−1) CP localized between the lithium and dihydrogen molecule indicates the interaction of the Li atom with the H_a atom. The geometric rearrangement of the atoms observed in the fifth step is mainly associated with the reorientation of the H_2 molecule with respect to the N−Li bond. In the $H_2NLi\cdots H_2$ complex (C_{2v}), the gradient path terminates at the (3,−1) CP of the hydrogen−hydrogen bond.

(b). Analysis of *s*(*ρ*). The NCI approach is associated with minima of $s(\rho)$ (i.e., repellors). Isorsurfaces of $s(\rho)$ are constructed around these minima, yielding the noncovalent

dx.doi.org/10.1021/jp4111376 | J. Phys. Chem. A 2014, 118, 1663−1672

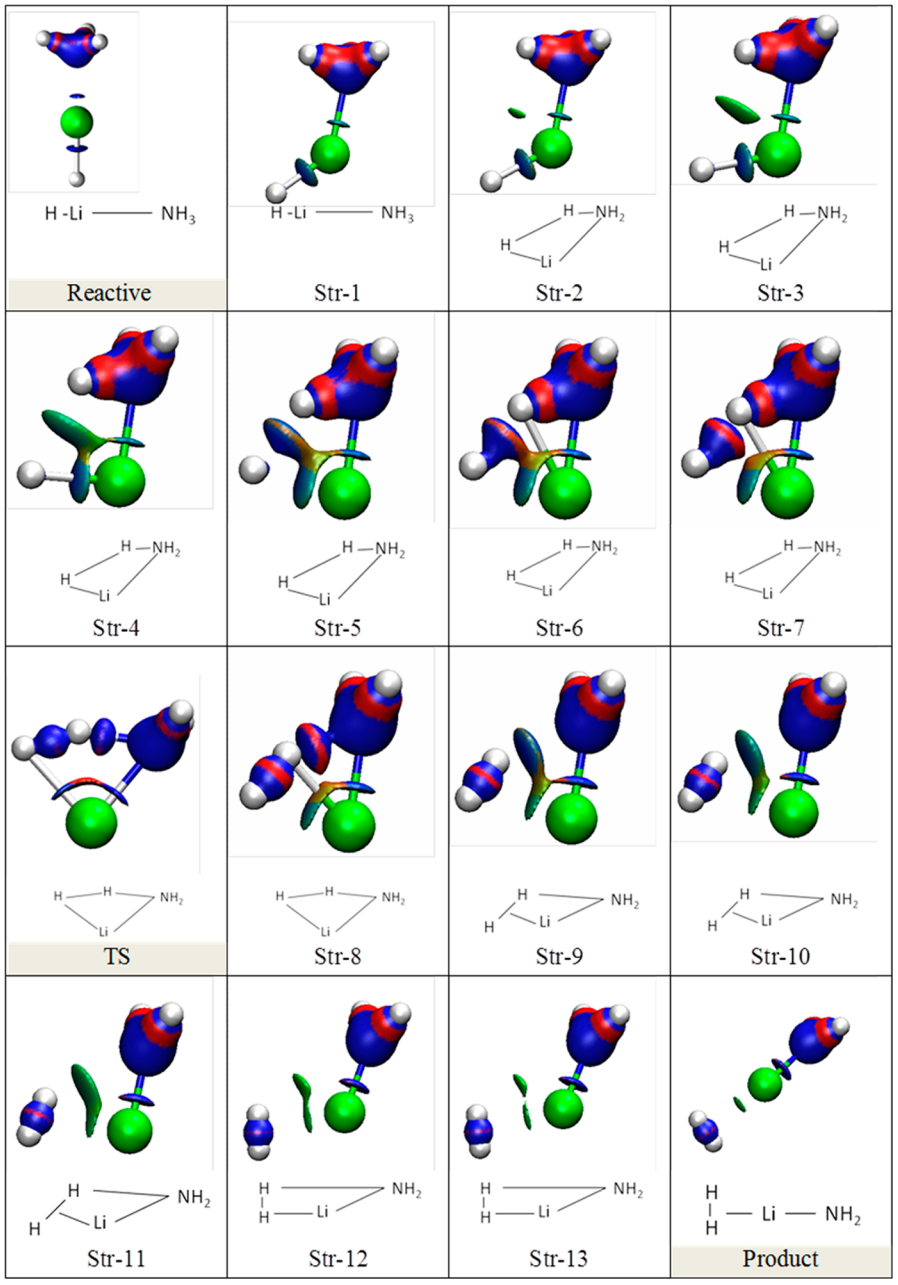

Figure 5. Reduced density gradient isosurfaces (s = 0.5 au) for different structures along the IRC path. The surfaces are colored on a blue−green−red scale according to values of sign (λ_2) of $\rho(r)$ over the range −0.05 to 0.05 au. Color blue indicates strong attractive interactions, and red indicates strong nonbonded overlap.

pattern of the molecule, which can be thought of as corresponding van der Waals, hydrogen bonds, steric repulsion, etc. Indeed, when the stationary points along the reaction are analyzed, the different noncovalent interactions present in each case are clearly revealed (see Figure 4) as follows:

- Reactive complex conformation ($LiH\cdots NH_3$): an isosurface is found around the noncovalent Li−N interaction, and another one for the ionic Li−H bond.
- Product complex conformation ($H_2\cdots LiNH_2$): the Li−N bond is maintained, though it is now weaker (greener), and a new noncovalent interaction has appeared between Li and the H_2 molecule. The H_a−H_b is not weak anymore, but covalent in nature.
- TS conformation: At the TS, both bonds are disappearing (Li−H_b and N−H_a), while the H_a−H_b bond is being formed. The Li−N bond, which is present in both the reactants and the products, appears to be of intermediate strength between both extreme cases.

It should be noted that in the stable conformations, a cutoff in the density of 0.05 suffices to find all the weak interactions in the system. However, along the reaction, breaking/forming processes take place, so that a greater cutoff is needed so that important features are not missed.[54] This explains the fact that N−H bonds are also observed in the TS configuration of Figure 4. Indeed, both noncovalent and covalent features can be revealed by means of the reduced density gradient.[32] It suffices

dx.doi.org/10.1021/jp4111376 | J. Phys. Chem. A 2014, 118, 1663−1672

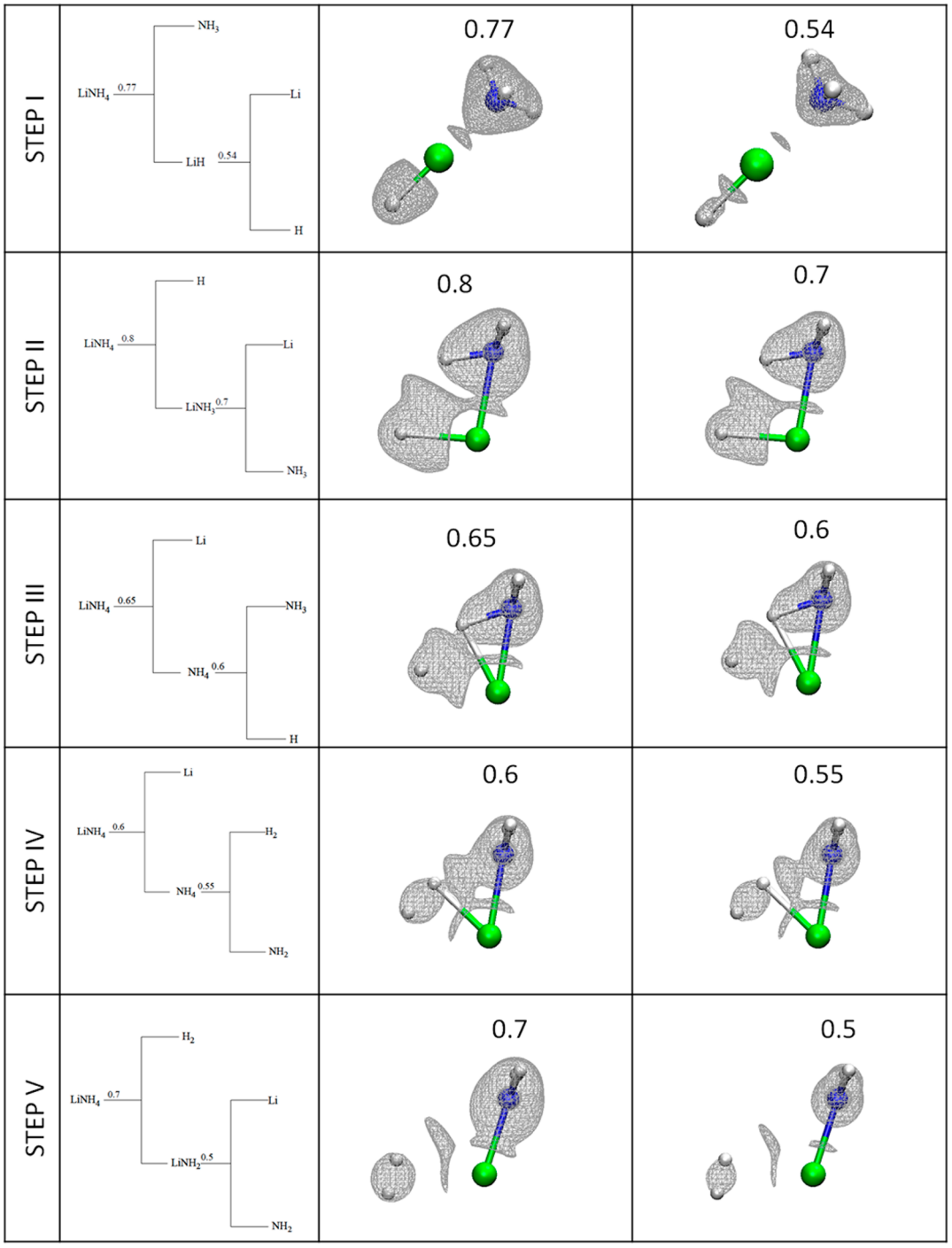

Figure 6. Bifurcation diagrams corresponding to the reduced density gradient analysis.

to use a higher cutoff (e.g., $\rho = 0.2$) so that all interactions are included in the analysis.

Figure 5 shows how noncovalent interactions evolve from the reactive conformation to the products, as in Figure 4, a cutoff of $\rho = 0.6$ has been used to include all interactions in the system (see Film in Supporting Information). Along the reaction, the new H−H interaction, though very weak, appears very soon and before the critical point in QTAIM. This is highlighted in Figure 4 by the use of several isosurface values: whereas QTAIM peaks appear at low values, pseudopeaks (peaks not going down to $s = 0$) require higher values to be visualized but enable to foresee QTAIM interactions such as the H−H. The appearance of this interaction marks the beginning of the transformation, as it is the bond that characterizes the product state. Indeed, along the reaction this interaction is progressively strengthened, while its respective isosurface becomes larger and bluer (see Figure 5 and Film in Supporting Information). As the TS becomes closer, all these interactions become more delocalized and form a unique surface (see Str-4, Figure 5). As will be shown later, this conformation is characteristic of atomic exchange (i.e., of the TS). Right before the TS we find an elongated N−H_a bond that is directed toward a deformed H_b atom and a delocalized interaction of these transition units with Li (see Str-7, Figure

dx.doi.org/10.1021/jp4111376 | J. Phys. Chem. A 2014, 118, 1663−1672

5). As the TS is reached, the N−H_a and the H_a−H_b bonds coexist. Right after the TS, the 3-body delocalized interaction is retrieved once again, though in this case the H_2 unit is already formed, so that the delocalized interaction encompasses the Li−N, N−H, and Li−H_2 interactions (see Str-9, Figure 5). This 3-body interaction evolves, favoring the Li−N and Li−H_2 bonds. First, the 3 interactions become isolated until the N−H interaction disappears and the product conformation is reached.

(c). Topology of $s(\rho)$: Bifurcation Trees. It has been observed that the interactions become delocalized around the TS. It would then be interesting to analyze the isosurface values that enclose all or just one interaction, i.e., analyze isosurfaces at different s values, also known as f-domains. Introduced by Mezey[55] within the Atoms in Molecules framework, the concept of an f-domain accounts for the volume enclosed by an isosurface of a value of $s = f$. When the system is partitioned from a chemically meaningful function's gradient, domains enable the characterization of basins according to common chemical knowledge. For example, f-domains have been extensively used within the ELF framework, enabling to recover the electron pair structure of a wide range of systems.[56] The limiting points (finite or infinite) of a field line are well-defined critical points, enabling to establish a relationship between real space points and the critical points. In both QTAIM and ELF, an ω-limit set is used: those points where the gradient lines arrive (attractors).[57] However, we have to keep in mind that within the NCI approach, interactions are associated with minima, i.e., where the gradient lines are born, so that we are dealing with an α-partition. Thus, as the value f decreases, successive splitting of the initial domains take place following the saddle points. This splitting, or reduction within the chemical topology jargon, takes place until all of the basins contain one and only one repellor or sink (please note, that the inverse behavior is observed in ELF, for example). Thus, the higher the value at the (3,+1) turning point, the weaker the relationship between the interaction is (e.g., in Figure 6-Step I, LiH and NH_3 form a less important unit Li and H, so its turning point is higher). When an isosurface contains more than one repellor, the domain is reducible, and as the value of $s(s)$ becomes lower, the domains split until a situation in which all domains are irreducible, i.e., we have one domain per repellor.

As the reduced gradient peaks are minima, surfaces are reduced going from high to low values. The value of $s(\rho)$ at which the reduction of domains takes place gathers a lot of information about the nature of the structure: if its bonds are localized the turning points will have a low value, whereas if the bonds are delocalized the turning point will have higher values. This is what is observed in our case. The reactive and product conformations show very clearly differentiated structures, with their respective units related to the reactive (LiH and NH_3) or the product ($LiNH_2$ and H_2) at high $s(\rho)$ values. Intermediate structures close to the TS, instead, show a continuous NCI surface around the valence even at low $s(\rho)$ values, what is know in topology as low persistence. Figure 6, for example, shows how the TS is divided into the reactive parts only at s = 0.6 (when the Li atom separates from the rest), and it is not until s = 0.47 that the bonds being formed and broken become irreducible domains.

Hence, we can say that the reduction of $s(\rho)$ domains describes the homogeneity in the $s(\rho)$ value. Since TSs are intrinsically associated with the bond formation/rupture process, this type of delocalized profiles are very characteristic f transition mechanisms as well as delocalized bonding types (such as π stacking). These delocalized situations are difficult to characterize with point-wise analysis (e.g., by mere critical point analysis), so that NCI provides a better picture of the bonding.[36]

4. COMPARISON

The reduced density gradient topology has shown to provide a rich and complementary information to the electronic density, enabling to smooth its profiles and criteria.

More specifically, the CPs in the field of $\rho(r)$ are characterized by a null density gradient. From eq 1, $s(\rho) = 0$ at the bond critical points, thus yielding a peak in the $s(\rho)$ diagram, and an associated isosurface in 3D. In other words, the process of bond formation and rupture coincides in their origin. However, changes within NCI are in many cases continuous (not catastrophic) and take place further in advance. The appearance of critical point in $\rho(r)$ is precluded in NCI by the appearance of a $s(\rho)$ peak that does not descend to $s = 0$. We can cite the appearance of the interaction H_a−H_b as an example in our reaction case. Thus, NCI foresees the results from topological analysis of $\rho(r)$ and can be used to predict the evolution of bonding patterns according to Bader theory. The appearance of pseudopeaks (peaks not related to ρ critical point) also enable to identify interactions beyond those present in QTAIM. This point has been recently highlighted in the literature for the analysis of weak intramolecular interactions.[44]

It should also be noticed that the use of the reduced density gradient isosurfaces enables a visual inspection of delocalized interactions, such as those involved in TSs.

5. CONCLUSIONS

A reaction mechanism is usually studied by finding reactants, products, intermediates, and TSs on the PES providing an adequate representation only based on energetic grounds. Alternatively, a chemical reaction can be studied from the redistribution of the electron density along the reaction path connecting the stationary points. The aim of this work is to describe the reaction mechanism by the structural evolution defined by the changes in the electron density during the chemical reaction. In this sense, it is possible to reveal the nature of the interactions that are present in the whole chemical process. Further development of the present strategy has the potential to deliver the reaction mechanism, defining the structure evolution and the sequence of bond breaking and bond formation by finding the structural changes and/or catastrophes.

Here, the molecular mechanism for the NH_3 + LiH → $LiNH_2$ + H_2 chemical reaction have been elucidated by topological analysis of the $\rho(r)$ and $s(\rho)$ functions, and it is represented by separated steps where respective bonds are broken and new ones are formed. Because the scalar fields are mutually not homeomorphic, therefore two different complementary pictures of the reaction are obtained.

It should be noted that this is the first time that the topology of $s(\rho)$ has been analyzed, taking into account not only its sinks[44] but also the saddle points for the construction of bifurcation trees. In these trees, several values of $s(\rho)$, instead of just one, are used in order to rank interaction types and identify their relationship.

We have shown that the NCI analysis can be considered as a global approach to QTAIM, which enables to recover its results, adding the following features: (i) Changes are not catastrophic. (ii) More interactions can be found, through the presence of pseudopeaks. (iii) Foresee interactions: the soft profile of NCI enables to predict the appearance of density critical points. (iv) Characterization of delocalized interactions: the use of surfaces beyond critical points enables to identify delocalized interactions, such as the ones involved in TSs.

Further works are currently ongoing to elucidate the molecular mechanism of complex chemical reactions involving a multibond-breaking/forming process.

An automated search of NCI critical points is being developed to automate the process.

■ ASSOCIATED CONTENT

Supporting Information

Additional information concerning complete ref 45 and a film supporting the transformation according to NCI index. This material is available free of charge via the Internet at http://pubs.acs.org.

■ AUTHOR INFORMATION

Corresponding Author

*(J.A.) E-mail: andres@qfa.uji.es.

Notes

The authors declare no competing financial interest.

■ ACKNOWLEDGMENTS

Financial support from Ministerio de Ciencia e Innovación (MICINN) for project CTQ-2012-36253-C03-01, Generalitat Valenciana for Prometeo/2009/053 project, and Universidad Jaume I-Fundación Bancaixa, project no. P1.1B2010-10 is gratefully acknowledged. The authors are also grateful to the Servei d'Informatica, Universitat Jaume I, and the Wroclaw Centre for Networking and Supercomputing for generous allocation of computer time. J.C.-G. thanks the CNRS for her position.

■ REFERENCES

(1) Chandler, D. Interfaces and the Driving Force of Hydrophobic Assembly. *Nature* **2005**, *437*, 640−647.

(2) Panigrahi, S. K.; Desiraju, G. R. Strong and Weak Hydrogen Bonds in the Protein−Ligand Interface. *Proteins* **2007**, *67*, 128−141.

(3) Hohenberg, P.; Kohn, W. Inhomogeneous Electron Gas. *Phys. Rev. B* **1964**, *136*, B864.

(4) Bader, R. F. W. *Atoms in Molecules: A Quantum Theory*; Clarendon Press: New York, 1990.

(5) Thom, R. Catastrophe Theory. *Nature* **1977**, *270*, 658−658.

(6) Becke, A. D.; Edgecombe, K. E. A Simple Measure of Electron Localization in Atomic and Molecular Systems. *J. Chem. Phys.* **1990**, *92*, 5397−5403.

(7) Silvi, B.; Savin, A. Classification of Chemical Bonds based on Topological Analysis of Electron Localization Functions. *Nature* **1994**, *371*, 683−686.

(8) Savin, A.; Jepsen, O.; Flad, J.; Andersen, O. K.; Preuss, H.; Vonschnering, H. G. Electron Localization in Solid State Structures of the Elements: The Diamond Structure. *Angwe. Chem., Int. Ed.* **1992**, *31*, 187−188.

(9) Krokidis, X.; Noury, S.; Silvi, B. Characterization of Elementary Chemical Processes by Catastrophe Theory. *J. Phys. Chem. A* **1997**, *101*, 7277−7282.

(10) Krokidis, X.; Vuilleumier, R.; Borgis, D.; Silvi, B. A Topological Analysis of the Proton Transfer in $H_5O_2^+$. *Mol. Phys.* **1999**, *96*, 265−273.

(11) Zeng, Y.; Meng, L.; Li, X.; Zheng, S. Topological Characteristics of Electron Density Distribution in SSXY → XSSY (X or Y = F, Cl, Br, I) Isomerization Reactions. *J. Phys. Chem. A* **2007**, *111*, 9093−9101.

(12) Li, X.; Fan, H.; Meng, L.; Zeng, Y.; Zheng, S. Theoretical Investigation on Stability and Isomerizations of CH_3SO Isomers. *J. Phys. Chem. A* **2007**, *111*, 2343−2350.

(13) Zeng, Y. L.; Zheng, S. J.; Meng, L. P. AIM Studies on Reactions FNCX → FXCN (X = O, S, and Se). *J. Phys. Chem. A* **2004**, *108*, 10527−10534.

(14) Zeng, Y. L.; Zheng, S. J.; Meng, L. P. Studies on Reactions INCX → IXCN (X = O, S, and Se). *Inorg. Chem.* **2004**, *43*, 5311−5320.

(15) Malcolm, N. O. J.; Popelier, P. L. A. On the Full Topology of the Laplacian of the Electron Density II: Umbrella Inversion of the Ammonia Molecule. *J. Phys. Chem. A* **2001**, *105*, 7638−7645.

(16) Polo, V.; Andres, J.; Castillo, R.; Berski, S.; Silvi, B. Understanding the Molecular Mechanism of the 1,3-Dipolar Cycloaddition between Fulminic Acid and Acetylene in terms of the Electron Localization Function and Catastrophe Theory. *Chem.—Eur. J.* **2004**, *10*, 5165−5172.

(17) Gonzalez-Navarrete, P.; Andres, J.; Berski, S. How a Quantum Chemical Topology Analysis Enables Prediction of Electron Density Transfers in Chemical Reactions. The Degenerated Cope Rearrangement of Semibullvalene. *J. Phys. Chem. Lett.* **2012**, *3*, 2500−2505.

(18) Gonzalez-Navarrete, P.; Domingo, L. R.; Andres, J.; Berski, S.; Silvi, B. Electronic Fluxes during Diels−Alder Reactions involving 1,2-Benzoquinones: Mechanistic Insights from the Analysis of Electron Localization Function and Catastrophe Theory. *J. Comput. Chem.* **2012**, *33*, 2400−2411.

(19) Berski, S.; Andres, J.; Silvi, B.; Domingo, L. R. New Findings on the Diels−Alder Reactions. An Analysis based on the Bonding Evolution Theory. *J. Phys. Chem. A* **2006**, *110*, 13939−13947.

(20) Alikhani, M. E.; Michelini, M. D. C.; Russo, N.; Silvi, B. Topological Analysis of the Reaction of Uranium Ions (U^+, U^{2+}) with N_2O in the Gas Phase. *J. Phys. Chem. A* **2008**, *112*, 12966−12974.

(21) Nizovtsev, A. S.; Kozlova, S. G. Electronic Rearrangements during the Inversion of Lead Phthalocyanine. *J. Phys. Chem. A* **2012**, *117*, 481−488.

(22) Nizovtsev, A. S. Activation of C−H bond in Methane by Pd Atom from the Bonding Evolution Theory Perspective. *J. Comput. Chem.* **2013**, *34*, 1917−1924.

(23) Suresh, C. H.; Koga, N.; Gadre, S. R. Revisiting Markovnikov Addition to Alkenes via Molecular Electrostatic Potential. *J. Org. Chem.* **2001**, *66*, 6883−6890.

(24) Balanarayan, P.; Kavathekar, R.; Gadre, S. R. Electrostatic Potential Topography for Exploring Electronic Reorganizations in 1,3 Dipolar Cycloadditions. *J. Phys. Chem. A* **2007**, *111*, 2733−2738.

(25) Fenniri, H.; Packiarajan, M.; Vidale, K. L.; Sherman, D. M.; Hallenga, K.; Wood, K. V.; Stowell, J. G. Helical Rosette Nanotubes: Design, Self-Assembly, and Characterization. *J. Am. Chem. Soc.* **2001**, *123*, 3854−3855.

(26) Kruse, P.; Johnson, E. R.; DiLabio, G. A.; Wolkow, R. A. Patterning of Vinylferrocene on H-Si(100) via Self-Directed Growth of Molecular Lines and STM-Induced Decomposition. *Nano Lett.* **2002**, *2*, 807−810.

(27) Fiedler, S.; Broecker, J.; Keller, S. Protein Folding in Membranes. *Cell. Mol. Life Sci.* **2010**, *67*, 1779−1798.

(28) Dill, K. A. Dominant Forces in Protein Folding. *Biochemistry* **1990**, *29*, 7133−7155.

(29) Silvi, B. Importance of Electrostatic Interactions between Nonbonded Molecules in Ice. *Phys. Rev. Lett.* **1994**, *73*, 842−845.

(30) Contreras-Garcia, J.; Calatayud, M.; Piquemal, J.-P.; Recio, J. M. Ionic Interactions: Comparative Topological Approach. *Comput. Theor. Chem.* **2012**, *998*, 193−201.

(31) Contreras-Garcia, J.; Johnson, E. R.; Keinan, S.; Chaudret, R.; Piquemal, J.-P.; Beratan, D. N.; Yang, W. NCIPLOT: A Program for

Plotting Non-Covalent Interaction Regions. *J. Chem. Theory. Comput.* **2011**, *7*, 625−632.
(32) Johnson, E. R.; Keinan, S.; Mori-Sanchez, P.; Contreras-Garcia, J.; Cohen, A. J.; Yang, W. Revealing Non-Covalent Interactions. *J. Am. Chem. Soc.* **2010**, *132*, 6498−6506.
(33) Contreras-Garcia, J.; Yang, W.; Johnson, E. R. Analysis of Hydrogen-Bond Interaction Potentials from the Electron Density: Integration of Non-Covalent Interaction Regions. *J. Phys. Chem. A* **2011**, *115*, 12983−12990.
(34) Sheiko, S. S.; Sun, F. C.; Randall, A.; Shirvanyants, D.; Rubinstein, M.; Lee, H.; Matyjaszewski, K. Adsorption-Induced Scission of Carbon−Carbon Bonds. *Nature* **2006**, *440*, 191−194.
(35) Di Labio, G. A.; Piva, P. G.; Kruse, P.; Wolkow, R. A. Dispersion Interactions Enable the Self-Directed Growth of Linear Alkane Nanostructures Covalently Bound to Silicon. *J. Am. Chem. Soc.* **2004**, *126*, 16048−16050.
(36) Saleh, G.; Gatti, C.; Lo Presti, L.; Contreras-García, J. Revealing Non-Covalent Interactions in Molecular Crystals through Their Experimental Electron Densities. *Chem.—Eur. J.* **2012**, *18*, 15523−15536.
(37) Gillet, N.; Chaudret, R.; Contreras-Garcia, J.; Yang, W.; Silvi, B.; Piquemal, J.-P. Coupling Quantum Interpretative Techniques: Another Look at Chemical Mechanisms in Organic Reactions. *J. Chem. Theory Comput.* **2012**, *8*, 3993−3997.
(38) Bader, R. F. W. Definition of Molecular Structure: By Choice or by Appeal to Observation? *J. Phys. Chem. A* **2010**, *114*, 7431−7444.
(39) Chen, P.; Xiong, Z. T.; Luo, J. Z.; Lin, J. Y.; Tan, K. L. Interaction of Hydrogen with Metal Nitrides and Imides. *Nature* **2002**, *420*, 302−304.
(40) Hu, Y. H.; Ruckenstein, E. H_2 Storage in Li_3N. Temperature-Programmed Hydrogenation and Dehydrogenation. *Ind. Eng. Chem. Res.* **2003**, *42*, 5135−5139.
(41) Hu, Y. H.; Ruckenstein, E. Ultrafast Reaction between LiH and NH_3 during H_2 Storage in Li_3N. *J. Phys. Chem. A* **2003**, *107*, 9737−9739.
(42) Kar, T.; Scheiner, S.; Li, L. Theoretical Investigation on the Mechanism of LiH + NH_3 → $LiNH_2$ + H_2 Reaction. *J. Mol. Struct.* **2008**, *857*, 111−114.
(43) Kalinowski, J.; Berski, S.; Latajka, Z. AIM and BET Approach for Ionic and Covalent Bond Evolution in Reaction of Hydrogen Elimination from Ammonia and Lithium Hydride. *Chem. Phys. Lett.* **2011**, *501*, 587−593.
(44) Lane, J. R.; Contreras-García, J.; Piquemal, J.-P.; Miller, B. J.; Kjaergaard, H. G. Are Bond Critical Points Really Critical for Hydrogen Bonding? *J. Chem. Theory. Comput.* **2013**, *9*, 3263−3266.
(45) Frisch, M. J.; Trucks, G. W.; Schlegel, H. B.; Scuseria, G. E.; Robb, M. A.; Cheeseman, J. R.; Scalmani, G.; Barone, V.; Mennucci, B.; Petersson, G. A.; et al. *Gaussian 09*, revision D.02; Gaussian, Inc.: Wallingford, CT, 2009.
(46) Becke, A. D. Density Functional Thermochemistry. 3. The Role of Exact Exchange. *J. Chem. Phys.* **1993**, *98*, 5648−5652.
(47) Becke, A. D. A New Mixing of Hartree−Fock and Local Density Functional Theories. *J. Chem. Phys.* **1993**, *98*, 1372−1377.
(48) Lee, C. T.; Yang, W. T.; Parr, R. G. Development of the Colle−Salvetti Correlation Energy Formula into a Functional of the Electron Density. *Phys. Rev. B* **1988**, *37*, 785−789.
(49) Dunning, T. H. Gaussian Basis Sets for use in Correlated Molecular Calculations. III. The Atoms Boron through Neon and Hydrogen. *J. Chem. Phys.* **1989**, *90*, 1007−1023.
(50) Hratchian, H. P.; Schlegel, H. B. Accurate Reaction Paths using a Hessian based Predictor Corrector Integrator. *J. Chem. Phys.* **2004**, *120*, 9918−9924.
(51) Keith, T. A.*AIMAll*, version 12.11.09; TK Gristmill Software: Overland Par, KS, 2012; aim.tkgristmill.com.
(52) Bieglerkonig, F. W.; Bader, R. F. W.; Tang, T. H. Calculation of the Average Properties of Atoms in Molecules. 2. *J. Comput. Chem.* **1982**, *3*, 317−328.
(53) Humphrey, W.; Dalke, A.; Schulten, K. VMD: Visual Molecular Dynamics. *J. Mol. Graphics* **1996**, *14*, 33−38.
(54) Chaudret, R.; de Courcy, B.; Contreras-Garcia, J.; Gloaguen, E.; Zehnacker-Rentien, A.; Mons, M.; Piquemal, J.-P. Unraveling Non-Covalent Interactions within Flexible Biomolecules: from Electron Density Topology to Gas Phase Spectroscopy. *Phys. Chem. Chem. Phys.* **2013**, DOI: 10.1039/C3CP52774C.
(55) Mezey, P. G. Quantum Chemical Shape: New Density Domain Relations for the Topology of Molecular Bodies, Functional Groups, and Chemical Bonding. *Can. J. Chem.* **1994**, *72*, 928−935.
(56) Calatayud, M.; Andrés, J.; Beltrán, A.; Silvi, B. The Hierarchy of Localization Basins: a Tool for the Understanding of Chemical Bonding Exemplified by the Analysis of the VO_x and VO_x^+ (x = 1−4) Systems. *Theor. Chem. Acc.* **2001**, *105*, 299−308.
(57) Teschl, G. *Ordinary Differential Equations and Dynamical Systems*; American Mathematical Society:Providence, RI, 2012.
(58) Salinas-Olvera, J. P.; Gómez, R. M.; Cortés-Guzmán, F. Structural Evolution: Mechanism of Olefine Insertion in Hydroformylation Reaction. *J. Phys. Chem. A* **2008**, *112*, 2906−2912.
(59) Cortés-Guzmán, F.; Gómez, R. M.; Rocha-Rinza, T.; Sánchez-Obregón, M. A.; Guevara-Vela, J. M. Valence Shell Charge Concentration (VSCC) Evolution: A Tool to Investigate the Transformations within a VSCC Throughout a Chemical Reaction. *J. Phys. Chem. A* **2011**, *115*, 12924−12932.

NOTE ADDED AFTER ASAP PUBLICATION

This paper was modified from the original version published on February 17, 2014 to include two additional references. The corrected version was published on February 19, 2014.